



1 **Black carbon (BC) in North Tibetan Mountain; Effect of**
2 **Kuwait fires on glacier**

3 Jiamao Zhou^{1,6}, Xuexi Tie^{1,2}, Baiqing Xu³, Shuyu Zhao¹, Mo Wang³, Guohui Li¹,
4 Song Yang³, Luyu Chang^{4,5}, Junji Cao¹

5 ¹KLACP, SKLLQG, Institute of Earth Environment, Chinese Academy of Sciences, Xi'an 710061,
6 China

7 ²Center for Excellence in Urban Atmospheric Environment, Institute of Urban Environment, Chinese
8 Academy of Sciences, Xiamen 361021, China

9 ³Key Laboratory of Tibetan Environment Changes and Land Surface Processes, Institute of Tibetan
10 Plateau Research, Chinese Academy of Sciences, Beijing 100101, China

11 ⁴Shanghai Meteorological Service, Shanghai, 200030, China

12 ⁵Shanghai Key Laboratory of Meteorology and Health, Shanghai, 200030, China

13 ⁶University of Chinese Academy of Sciences, Beijing 100049, China

14 *Correspondence to:* Xue Xi Tie (tiexx@ieecas.cn) or Baiqing Xu (baiqing@itpcas.ac.cn)

15

16

17



18 **Abstract.** The BC deposition on the ice core at Muztagh Ata Mountain, Northern Tibetan Plateau was
19 analyzed. Two sets of measurements were used in this study, which included the air samplings of BC
20 particles during 2004-2006 and the ice core drillings of BC deposition during 1986-1994. Two
21 numerical models were used to analyze the measured data. A global chemical transportation model
22 (MOZART-4) was used to analyze the BC transport from the source regions, and a radiative transfer
23 model (SNICAR) was used to study the effect of BC on snow albedo. The results show that during
24 1991-1992, there was a strong spike of the BC deposition at Muztagh Ata, suggesting that there was an
25 unusual emission in the upward region during this period. This high peak of BC deposition was
26 investigated by using the global chemical transportation model (MOZART-4). The analysis indicated
27 that the emissions from large Kuwait fires at the end of the first Gulf War in 1991 caused this high peak
28 of the BC concentrations and deposition (about 3-4 times higher than other years) at the Muztagh Ata
29 Mountain, suggesting that the upward BC emissions had important impacts on this remote site located
30 in Northern Tibetan Plateau. Thus, there is a need to quantitatively estimate the effect of surrounding
31 emissions on the BC concentrations in the northern Tibetan Plateau. In this study, a sensitive study with
32 4 individual BC emission regions (Central Asia, Europe, Persian Gulf, and South Asia) was conducted
33 by using the MOZART-4 model. The result suggests that during the “normal period” (non Kuwait
34 Fires), the largest effect was due to the Central Asia source (44%) during Indian monsoon period, while
35 during non-monsoon period, the largest effect was due to the South Asia source (34%). The increase of
36 radiative forcing increase (RFI) due to the deposition of BC on snow was estimated by using the
37 radiative transfer model (SNICAR). The results shows that under the fresh snow assumption, the
38 estimated increase of RFI ranged from 0.2 W m^{-2} to 2.5 W m^{-2} , while under the aged snow assumption,
39 the estimated increase of RFI ranged from 0.9 W m^{-2} to 5.7 W m^{-2} . During the Kuwait fires period, the
40 RFI values increased about 2-5 times higher than the “normal period”, suggesting a significant increase
41 for the snow melting in Northern Tibetan Plateau due to this fire event. This result suggests that the
42 variability of BC deposition at the Muztagh Ata Mountain provides useful information to study the
43 effect of the upward BC emissions on environmental and climate issues in the Northern Tibetan Plateau.
44 The radiative effect of BC deposition on the snow melting provides important information regarding
45 the water resources in the region.

46

47 **Key Words; Northern Tibetan glaciers, BC deposition, MOZART model**

48



49 1 Introduction

50 Black carbon (BC) particles emitted from combustion are considered as an important air pollutant, as
51 they change the radiative balance of the atmosphere directly by absorbing and scattering solar radiation,
52 and indirectly by changing the microphysical process of cloud (acting as ice nuclei) and precipitation
53 efficiency (acting as cloud condensation nuclei) (Ramanathan et al., 2001). Albedo changes induced by
54 strongly light absorbing component by deposited on the surface of snow and ice are the key parameters
55 to determine radiative forcing and accelerate melting (Holben et al., 1998; Hansen and Nazarenko,
56 2004). Due to the strong regional to local distribution of BC, these properties are not well understood,
57 particularly in remote regions, such as the Tibetan Plateau.

58

59 BC particles can deposit and preserve in the ice by the progress of post-deposition on the glaciers and
60 ice sheets. Retrieved ice cores from remote mountain glaciers and ice sheets provide useful information
61 of the historical BC aerosol emissions and synchronous meteorology conditions. Previous studies on
62 records of carbonaceous aerosols show that the emissions of fossil fuel combustion from Central
63 Europe had significant impact on the glacier in the Swiss Alps (Lavanchy et al., 1999). Ice cores drilled
64 from Antarctica suggest that the Southern Hemisphere biomass burning were strongly influenced by
65 continental hydrology (Bisiaux et al., 2012). McConnell et al. (2007) differentiated the BC emissions
66 from industrial activities and forest fires using an ice core in Greenland. These researches indicate that
67 BC records in history are important and practicable method to investigate the regional aerosol transport
68 and emission variations.

69

70 In this study, the ice core BC at Muztagh Ata, Northern Tibetan Plateau is analyzed. Identification the
71 source regions, which have important impact on BC deposition at Muztagh Ata is very important
72 scientific issue, because of its location. In particularly, there was a strong spike of the BC deposition
73 during 1992-1993 at Muztagh Ata (as shown in the following text), reflecting that there was unusual
74 emission in the upward region from Muztagh Ata. This strong spike of the ice core BC was about 3-4
75 times higher than other years, producing important effects on climate and hydrological cycle. As a
76 result, the study of the sources of BC, which affect the ice core BC in this location, needs to be
77 carefully studied. Muztagh Ata locates in the east of Pamir and the north of Tibetan Plateau. The ice
78 core data provides important information for atmospheric circulation and climate change in Asia (An et
79 al., 2001). Moreover, the climate in Muztagh Ata is very sensitive to solar warming mechanisms
80 because it has a large snow cover in the region, resulting in important impacts on the hydrological cycle
81 of the continent by enhancing glacier melt.

82

83 The BC sources which contribute the BC deposition in Tibetan Plateau have been previously studied.
84 Their results show that BC deposited on glaciers in the Pamir Mountains was originated from Europe,
85 Middle East and central Asia (Liu et al., 2008; Xu et al., 2009a; Wang et al., 2015b), whereas BC
86 deposited on glaciers over the Himalayas and southeastern Tibetan Plateau was mainly affected by the
87 western upward regions in winter. During the Indian summer monsoon season, they were mainly
88 affected by the BC sources in Indian region (Ming et al., 2008; Xu et al., 2009b; Kaspari et al., 2011;



89 Wang et al., 2015a). However, at present, the effects of the transport pathways and individual
90 contributions of BC sources to the Muztagh Ata region have not been carefully studied. Because the
91 radiative forcing caused by BC in snow and ice between different regions is very different, depending
92 upon the emitting intensities, ocean-land distributions, topography, regional atmospheric circulations,
93 and other factors, detailed study on the source contributions to the region as well as the climate effect
94 are needed to carefully study this important region.

95
96 Both the ice core deposition measurements at Muztagh Ata and a global chemical model (MOZART-4;
97 Model for Ozone and Related chemical Tracers, version 4) are used in this study. To better evaluate the
98 model performance, the air samples of BC particles during 1986-1994 were also analyzed. The global
99 chemical transport model (MOZART-4) was used to analyze the long-term trend in the early 90s of the
100 observed BC deposition and to quantify the individual contribution of different BC sources to the
101 deposition on the snow cover. The modeled temporal variations and magnitude of the BC
102 concentrations in the atmosphere and snow were compared to observations. Finally, a radiative transfer
103 model (SNICAR) was used to study the effect of BC on snow albedo, radiative forcing, and runoff
104 changes induced by the BC deposition on the Muztagh Ata snow.

105

106 **2 Methodologies**

107 **2.1 Sampling Sites**

108 Muztagh Ata Mountain is located in the north side of Tibetan Plateau. Both atmospheric sampling and
109 ice core drilling BC were conducted at the Muztagh Ata site. The atmospheric sampling BC
110 (38°17.30'N, 75°01.38'E) was conducted by the Cold and Arid Regions Environmental and
111 Engineering Institute, Chinese Academy of Sciences, at a 4500 m above sea level (a.s.l.). A 170.4 m ice
112 core (9.5 cm in diameter) was drilled during the summer season in 2012 from Kuokuosele (KKSL)
113 Glacier of Muztagh Ata (38°11'N, 75°11'E, 5700 m a.s.l.), which was conducted by the Institute of
114 Tibetan Plateau Research, Chinese Academy of Sciences. Because the site is surrounded by several
115 important BC source regions, this measurement site is suitable to investigate the effect of BC emissions
116 on north part Tibetan Plateau, which plays important roles for global climate and hydrology (see Fig.
117 1).

118

119 The average annual temperature at the peak of the mountain is approximately -20°C. Because the
120 numerous high mountains block the warm and humid air currents from Indian and Pacific Ocean, the
121 climate in this area is relatively dry. The averaged annual precipitation is less than 200 mm, which is
122 mainly snow to form perennial glaciers. There are 128 modern glaciers and on average about 377
123 square kilometers. The prevailing winds in this region are usually westerly jet stream. Previous studies
124 suggested that there was very small effect by local sources, and the aerosol pollutions were originated
125 mainly from the west by mid- and long-range transport. During summer, the South Asia monsoon had
126 also important effect on the transport of BC particles from India (Liu et al., 2008; Wu et al., 2008; Zhao



127 et al., 2011; Wang et al., 2015b).

128

129 2.2 Measurements

130

131 During the period from December 5, 2003 to February 17, 2006, Eighty-one valid total suspended
132 aerosol particle (TSP) and BC samples were obtained. The measurements were conducted under very
133 difficult environmental conditions, because of its high mountain location. The sample numbers for
134 spring, summer, autumn, and winter was 19, 21, 14, 27, respectively. Each sample was collected over
135 one week and on 15 mm Whatman quartz microfibre filter (QM/A, Whatman LTD, Maidstone, UK),
136 which was pre-combusted at 800°C for 3 hours to remove the potential carbon disturbance.

137

138 For the ice core measurement, a 170.4 m ice core (9.5 cm in diameter) was drilled during the summer
139 season in 2012 from Kuokuosele (KKSL) Glacier of Muztagh Ata (38°11'N, 75°11'E, 5700 m a.s.l.),
140 which is close to the BC air sampling site. A 3-mm outer layer of the ice sections was removed with a
141 pre-cleaned stainless steel scalpel at -5°C in a class 100 laminar flow bench to eliminate contamination
142 that may have occurred during drilling, transport, and storage. The inner section for BC analysis was
143 sealed in a 50 ml polypropylene vial (BD Falcon, cat. no. 358206). The ice core dating and calculation
144 of BC deposition fluxes were provided by Institute of Tibetan Plateau Research, Chinese Academy of
145 Science. The detailed method for the measurement of BC deposition is shown by Xu et al. (2009a).

146

147 2.3 Measurements and analytical methods

148

149 The elemental carbon (EC, which is proxy to BC in this study) analyses for atmospheric filters were
150 carried out by using Desert Research Institute (DRI) Model 2001 carbon analyzer (Atmoslytic Inc.,
151 Calabasas, CA, USA) with IMPROVE (Interagency Monitoring of PROtected Visual Environments)
152 thermal/optical reflectance (TOR) protocol (Chow et al., 1993; Chow et al., 2004). A 0.526 cm² punch
153 of a quartz filter sample was heated in a stepwise manner to obtain data for three elemental carbon (EC)
154 fractions (EC1, EC2, and EC3 in a 2% oxygen/98% helium atmosphere at 580, 740, and 840 °C. At the
155 same time, OP (pyrolyzed carbon) was produced at <580 °C in the inert atmosphere which decreases
156 the reflected light to correct for charred OC. Total EC is the sum of the three EC fractions minus OP.
157 More details and QAQC (Quality Assurance and Quality Control) are shown by Cao et al. (2003) and
158 Cao et al., (2009).

159

160 The rBC (refractory black carbon), which is used instead of BC for measurements derived from
161 incandescence methods (Petzold et al., 2013), was analyzed at Institute of Tibetan Plateau Research,
162 Chinese Academy of Sciences by using a Single Particle Soot Photometer (SP2) coupled with an
163 ultrasonic nebulization system (CETAC UT5000). The laser-induced incandescence was used to
164 measure the mass of rBC in individual particles (Schwarz et al., 2006). The incandescence signal can
165 be converted to rBC mass which is detected by photomultiplier tube detectors. This analytical method
166 was previously applied to ice cores by several studies ((McConnell et al., 2007; Kaspari et al., 2011;



167 Bisiaux et al., 2012). Detailed description on the SP2 analytical process and calibration procedures can
168 be found in (Wendl et al., 2014) and (Wang et al., 2015b).

169

170 Although the differences in the two analytical techniques (Wang et al., 2015b), in order to facilitate the
171 discussions, they are uniformly referred to as black carbon (BC) in our study since both of them are
172 materials share some of the characteristics of BC with its light-absorbing properties (Petzold et al.,
173 2013).

174

175 **2.4 Global chemistry transport model / MOZART-4**

176

177 The model used in this study is MOZART-4 (Model for Ozone and Related chemical Tracers, version
178 4). The model is an offline global chemical transport model for the troposphere developed jointly by
179 the National Center for Atmospheric Research (NCAR), the Geophysical Fluid Dynamics Laboratory
180 (GFDL), and the Max Planck Institute for Meteorology (MPI-Met). The detailed model description and
181 model evaluated can be found in Emmons et al. (2010). The aerosol modules was developed by Tie et
182 al. (2005). This model have been developed and used to quantify the global budget of trace gases and
183 aerosol particles, and to study their atmospheric transport, chemical transformations and removal
184 (Emmons et al., 2010; Chang et al., 2016). The model is built base on the framework of the Model of
185 Atmospheric Transport and Chemistry (MATCH) (Rasch et al., 1997). Convective mass fluxes are
186 diagnosed by using the shallow and mid-level convective transport formulation of Hack (Hack, 1994)
187 and deep convection scheme (Zhang and McFarlane, 1995). Vertical diffusion within the boundary
188 layer is built on the parameterization by Holtslag and Boville (1993). Advective transport scheme used
189 the flux form semi-Lagrangian transport algorithm (Lin and Rood, 1996). The wet deposition includes
190 in-cloud as well as below-cloud scavenging developed by Brasseur et al. (1998) is taken into
191 MOZART-4. Details of the chemical solver scheme can be found in the Auxiliary Material (Kinnison
192 et al., 2007).

193

194 In the present study, the model includes 85 gas-phase species, 12 bulk aerosol compounds and
195 approximately 200 reactions. The horizontal resolution of this study is $1.9^{\circ} \times 2.5^{\circ}$ with 56 hybrid
196 sigma-pressure vertical levels from the surface to approximately 2 hPa. The meteorological initial and
197 boundary conditions are down load from NCAR Community Data Portal (CDP), using National
198 Centers for Environmental Prediction (NCEP) meteorology. The model transport of this study is driven
199 by the Modern-Era Retrospective-analysis for Research and Applications (MERRA) 6-hour reanalysis
200 data with a $1.9^{\circ} \times 2.5^{\circ}$ grid provided by National Aeronautics and Space Administration (NASA).

201

202 The BC emission inventory used in this global model is based on the simulation of the POET
203 (Precursors of Ozone and their Effects in the Troposphere) database from 1997 to 2007 and the data of
204 BC emission inventory including fossil fuel and biofuel combustion from a previous study (Bond et al.,
205 2004; Bond et al., 2007). Figure 2 illustrates the updated 21-year average global BC emissions from
206 1986 to 2006. There are two types of black carbon particles in MOZART-4, hydrophobic and



207 hydrophilic particles. Hydrophobic particles are directly emitted from the sources, and are converted to
208 hydrophilic in the atmosphere (Hagen et al., 1992; Liousse et al., 1993; Parungo et al., 1994), with a
209 rate constant of $7.1 \times 10^{-6}/s$ (Cooke and Wilson, 1996).

210

211

212 2.5 BC deposition estimation

213

214 In order to compare to the measured ice core BC deposition at the Muztagh Ata Mountain, the BC
215 deposition flux is calculated in this study. In the estimation, the calculated atmospheric BC
216 concentrations and precipitation data obtained from China Meteorological Data Service Center were
217 compiled and evaluated. In addition, annual BC deposition parameters and deposition flux calculation
218 methods were described in other studies (Jurado et al., 2008; Yasunari et al., 2010; Fang et al., 2015; Li
219 et al., 2017). In brief, deposition fluxes are calculated by the following equations:

220

$$221 F_{DD} = 10^{-4} v_D C_{BC} t \quad (1)$$

$$222 F_{WD} = 10^{-7} p_0 W_p C_{BC} \quad (2)$$

$$223 F_{BC} = F_{DD} + F_{WD} \quad (3)$$

224

225 where 10^{-4} and 10^{-7} are unit conversion factors; F_{DD} and F_{WD} are the annual dry and wet deposition
226 (ng cm^{-2}), respectively; the total BC deposition flux (F_{BC}) (ng cm^{-2}) is the sum of F_{DD} and F_{WD} ; where
227 v_D (m s^{-1}) is the dry deposition velocity of black carbon; t is total estimation time for one year (s);
228 p_0 is the annual precipitation rate (mm); W_p is the particle washout ratio (dimensionless); and C_{BC}
229 is the annual atmospheric BC concentrations at Muztagh Ata Mountain (ng m^{-3}). There are large
230 differences in estimates on v_D and W_p (Jurado et al., 2005; Jurado et al., 2008; Yasunari et al., 2013).
231 A fixed small dry deposition velocity of $1.0 \times 10^{-4} \text{ m s}^{-1}$ onto snow was adopted (Yasunari et al., 2010;
232 Nair et al., 2013) and the corresponding estimation values are likely to represent a lower bound for BC
233 dry deposition in this area. Particle washout ratio W_p is assumed to be a constant and equal to 2×10^5
234 which has been adopted in many modeling exercises and fits well with field measurements (Mackay et
235 al., 1986; Jurado et al., 2005; Fang et al., 2015; Li et al., 2017).

236 3 Results and discussion

237 3.1 Model evaluation and compared to observation

238

239 In order to better understand the variation, characteristics, and source contributions of the BC
240 concentrations at Muztagh Ata Mountain, model sensitive studies using MOZART-4 were conducted in
241 this study. Firstly, the model was evaluated by comparing the observed monthly BC concentrations
242 with the calculated monthly BC concentrations during January 2004 to February 2006. As shown in Fig
243 3a, the simulated BC concentrations had a similar magnitude of measured BC concentrations, with
244 mean values of 62.4 ng m^{-3} and 56.5 ng m^{-3} for the calculation and measurement, respectively. There



245 was also evident that the measured variability of BC was captured by the calculation. For example, the
246 calculated variability was comparable to the measured result between July 2014 and Oct. 2015.
247 However, some differences were also noticeable. For example, the calculated BC concentration was
248 overestimated in the winter of 2004 and underestimated in the winter of 2006. Because the measured
249 site locates in a “clean” region of BC emission, the BC particles were mostly transported from
250 long-distance of the upwind regions. There were uncertainty related to the emissions and simulated
251 meteorological parameters (wind speeds, wind directions, etc.). As a result, it caused the discrepancy
252 between calculated and measured BC concentrations at the Muztagh Ata Mountain. There was another
253 reason may cause the difficulty of the calculation. The horizontal resolution of the global model is
254 relatively low ($1.9^{\circ} \times 2.5^{\circ}$ in this study), which is unable to reproduce some detailed variability in the
255 simulation. However, the overall features of the measured BC concentrations were reproduced by the
256 model, such as the magnitude and seasonal variability (see Fig. 3b), suggesting that the model is
257 capable to study long-range transport from BC source regions to the remote site.

258

259 The simulated seasonal variation shows in Fig 3b. The result shows that calculated seasonal variation
260 was generally agreed with the measured variation, except the value in spring. According to the analysis
261 of the source contribution (shown in Section 3.3), the BC emission in South Asia has significant
262 contributions to the BC concentrations at Muztagh Ata during non-summer season which accounted for
263 average 31~60% in spring and few contributions in summer season. The overestimated BC
264 concentrations may due to the fact that the model overestimated the pollutant transportation from the
265 emission sources to sampling site crossing the high mountains of Tibet Plateau, which act as a wall to
266 block the transportation from the BC emission in South Asia to the sampling area (Zhao et al., 2013).

267

268 3.2 Long-term Ice core measurement and possible effect of Kuwait fire event

269

270 In addition to the atmospheric sampling of BC measurement, there is a long-term ice cores
271 measurement of BC at the Muztagh Ata Mountain. This long-term measurement represents a valuable
272 data to show the long-term trend and inter-annual variability. Ice core records obtained at Muztagh Ata
273 Mountain are irreplaceable when evaluating contemporary atmospheric or snow BC concentration
274 variations. A long-term ice-core measurement (from 1940 to 2010) was provided by Xu et al. at
275 Muztagh Ata Mountain. Their results showed that the ice core BC concentrations were between 0.30
276 and 39.54 ng g^{-1} from 1940 to 2010, with an average value of 7.22 ng g^{-1} . The BC deposition fluxes
277 were between 9.96 and 909.88 ng cm^{-2} , with an average of 184.18 ng cm^{-2} . It is interesting to note that
278 both BC concentration and BC deposition of ice core showed a sharply increase in 1992, which was
279 about five times higher than the average mean value as shown in Fig 4. No other similar peak was
280 found in the entire record which may indicate a specific event to lead to this sharp increased, which
281 provide useful information to track the BC emissions. In this study, we conduct several model studies
282 to investigate this special event.

283

284 As shown in Figure 4, there was a high BC deposition flux (900 ng cm^{-2}) in 1992, compared to 100-300



285 ng cm^{-2} in other years. In order to investigate this special event, we focus our model study on a short
286 period (from 1986 to 1994). One potential reason to cause this sharp increase of BC was that during
287 1991, when Iraqi troops withdrew from Kuwait at the end of the first Gulf War, they setted a huge fire
288 over 700 oil wells. The fires were started in January and February 1991, and the last well was capped
289 on November 6, 1991. The resulting fires produced a large plume of smoke and particles that had
290 significant effects on the Persian Gulf area and the potential for global effects (as shown in Fig. 5).

291

292 In order to estimate intensive of the BC emission from the fires, (Hobbs and Radke, 1992) conducted
293 two aircraft studies during the period 16 May through 12 June 1991 to evaluate the effects of the smoke.
294 The estimated emission rate of elemental carbon of the Kuwait fires is ~ 3400 metric tons per day which
295 is 13 times the BC emissions from all U.S. combustion sources in total.

296

297 In order to the effect of the huge Kuwait fires on the BC ice core deposition, the MOZART-4 model
298 was applied to simulate the atmospheric BC concentrations and deposition fluxes variation from 1986
299 to 1994. Several model sensitive studies were conducted. First, the atmospheric BC concentration was
300 calculated by the anthropogenic BC emission with the default emissions (POET) as described before.
301 Second, in order to simulate the large increase in the BC emissions caused by the Kuwait fires in
302 Persian Gulf (Region 3 in Fig. 1), according to the measured values of Hobbs and Radke (1992), the
303 BC emissions were significantly enhanced by 50 times from January to November, 1991 to represent
304 Kuwait fires. Figure 4 shows the horizontal distribution of the calculated BC plume from the Kuwait
305 fires, with the enhanced BC emission.

306

307

308 The calculated result suggests that there was a significant increase of BC concentrations nearby the
309 Kuwait fires (see Fig. 6). The BC concentrations reached to $10\text{--}20 \mu\text{g m}^{-3}$ at the surface (see Fig. 6A)
310 and more than $0.7 \mu\text{g m}^{-3}$ at 5 km above the surface (see Fig. 6B). As shown in Figs. 5 and 6, the winds
311 nearby the fire region were toward to northern and northwestern directions. Because the lifetime of
312 black carbon aerosols is sufficiently long (about a week) (Ramanathan et al., 2001; Bauer et al., 2013),
313 the high BC concentrations were transported westerly toward the Muztagh Ata Mountain.

314

315 The evaluation of the modeled BC deposition at the Muztagh Ata Mountain was conducted by
316 comparison between the calculation and measurement (see Fig. 4). Figure 4 shows the calculated
317 temporal variation of BC concentrations and deposition, which were compared with the measured
318 variations. The result shows that the calculated temporal variability of BC deposition was generally
319 consistent with the measured variability. For example, the both high peaks of calculated and measured
320 BC deposition occurred in 1992. The calculated atmospheric concentrations of BC, however, had a
321 peak value in 1991. This was due to the fact that the deposition of BC in ice core was an accumulated
322 value, while the atmospheric BC concentration was an in-situ value. Despite of the consistence of
323 temporal variations between measured and calculated deposition of BC, there was a consistent
324 underestimate of calculated BC deposition compared to the measured value. Because there were



325 uncertainties in estimates BC emission and the deposition, these uncertainties could result in the
326 discrepancy between the calculation and measurement. For example, according to the assimilation
327 meteorological data by Chinese Meteorological Administration, the annual precipitation in 1992 was about
328 twice higher than in 1991 nearby Muztagh Ata Mountain, suggesting that scavenging efficiency may
329 likely underestimated, causing the calculated uncertainty in the estimate of the BC deposition.

330

331 **3.3 Effect of regional BC emissions at the Muztagh Ata Mountain**

332

333 To further understand the influence of transportation and deposition on the annual variation of BC at
334 the Muztagh Ata Mountain (as a receptor region), sensitivity experiments using the MOZART-4 model
335 were conducted. In the sensitive study, the effect of different BC emission regions on the BC
336 concentrations at the measurement site was individually calculated. Four primary regions were defined
337 as shown in Table 1 and Fig. 1, including (R1) Central Asia, (R2) Europe, (R3) Persian Gulf, and (R4)
338 South Asia. In each sensitive study, only the individual BC emission was included, and the BC
339 emissions in other regions were excluded. As a result, the fractional contributions by the individual
340 emission regions to BC concentrations in the receptor region (the Muztagh Ata Mountain) were
341 calculated. Table 1 shows the calculated results.

342

343 In order to clearly show the transport pathways from the different regions to the measurement site and
344 the Tibetan Plateau, the calculated horizontal distributions of BC concentrations from each region
345 during 3 different periods (summer monsoon, non-monsoon, and annual mean) were shown in Fig. 7.

346

347 The results from Table 1 and Fig. 7 suggests that during the “normal period” (non Kuwait Fires), the
348 BC emissions from Central Asia and South Asia had the largest contributions to the BC concentrations
349 at measurement site, contributing annual mean of 27% and 25%, respectively. It is interesting to note
350 that there were strong seasonal variations regarding the effects. During the monsoon period, the largest
351 effect was due to the Central Asia source (44%), while during non-monsoon period, the largest effect
352 was due to the South Asia source (34%).

353

354 As shown in Fig. 7, during the monsoon period, the airflow from the oceans (Persian Gulf and Bengal
355 Bay) moves northward and coupled with the strong precipitation. As a result, the BC particles from
356 south Asian source were washout during the transport pathway, leading to lower BC concentrations at
357 the measurement site. In contrast, during the non-monsoon period, the prevailing winds were western
358 winds, which BC emission in the northern India was transported to the measurement site measurement
359 site, leading to higher BC concentrations. The contributions from Persian Gulf emissions were
360 generally low to the BC concentrations. However during Kuwait fires period, this region had
361 significant contribution to the Muztagh Ata area as well as the Tibetan Plateau.

362

363 **3.4 Radiative forcing induced by BC in Muztagh Ata glacier**

364



365 The deposition of BC on the snow reduces the surface albedo, causing a positive radiative forcing and
366 increases in ice and snow melt. Previous studies show that BC particles produce significant reduction in
367 the snow albedo, with the solar visible wavelengths (Warren and Wiscombe, 1980). In this study, the
368 effect of BC deposition on the snow albedo and radiative forcing during 1986 to 1994 in Muztagh Ata
369 glacier was estimated. The SINICAR model (Snow, Ice, and Aerosol Radiation; available at
370 <http://snow.engin.umich.edu>) was used to estimate the effect of BC particles on snow albedo in
371 different solar wavelengths (Flanner and Zender, 2005; Flanner et al., 2007).

372

373 To estimate the effect of the BC deposition on surface albedo, in addition to the BC concentrations,
374 there are several environmental factors such as snow grain size, solar zenith angle, and snow depth
375 were needed to be estimated (Warren and Wiscombe, 1980). The setup of input parameters required for
376 running the SNICAR model is briefly described as below. As we focus on the calculation of radiative
377 forcing caused by BC particles, other impurity contents, such as dust and volcanic ash, were set to be
378 zero. A mass absorption cross section (MAC) of $7.5 \text{ m}^2 \text{ g}^{-1}$ at 550 nm for uncoated BC particles (Bond
379 and Bergstrom, 2006) was assumed to be same as the default value, and the MAC scaling factor in the
380 online SNICAR model as one of input parameters was set to be 1.0. The effective radius of $100 \mu\text{m}$
381 with a density of 60 kg m^{-3} was used for new snow, and the effective radius of $400 \mu\text{m}$ with a density of
382 400 kg m^{-3} was adopted for the albedo estimation according to the previous studies and measurements
383 in other studies in Tibetan Plateau (Wiscombe and Warren, 1980; Wu et al., 2006). The extractive snow
384 height from MERRA (the Modern-Era Retrospective-analysis for Research and Applications)
385 reanalysis products was used for snowpack thickness. The forcing dataset used in this study was
386 developed by Data Assimilation and Modeling Center for Tibetan Multi-spheres, Institute of Tibetan
387 Plateau Research, Chinese Academy of Sciences (Chen et al., 2011). The recovered BC concentrations
388 of ice core were used as the input parameter of uncoated black carbon concentration. The averaged
389 short-wave flux and solar zenith angle of each month were obtained from China Meteorological
390 Forcing Dataset provided by Data Assimilation and Modeling Center for Tibetan Multi-spheres,
391 Institute of Tibetan Plateau Research, Chinese Academy of Sciences.

392

393 The measured average BC concentration in ice core during 1986-1994 was 15.2 ng g^{-1} , with a peak
394 value of 39.2 ng g^{-1} . The calculated snow albedo reduction by using the SNICAR model ranged from
395 0.11% to 1.36% by assuming that the snow layer was totally covered by fresh snow (lower limit).
396 However, if it was aged layer, the estimated snow albedo reduction increased, ranging from 0.47% to
397 2.97% (upper limit). The actual value should be lied between the two ranges. This result is consistent
398 with the previous studies. For example, (Yasunari et al., 2010) reported that the reduction of snow
399 albedo ranged from 2.0% to 5.2%, with the BC concentration of 26.0-68.2 ng/g, based on atmospheric
400 BC measurements at NCO-P over the southern slopes of western Himalayas.

401

402 The reduction of snow albedo enhanced the absorption of solar energy and accelerated snow and ice
403 melt (Conway et al., 1996). Several studies suggested that that BC containments on snow were very
404 effective to reduce the surface albedo (Warren and Wiscombe, 1980; Petr Chylek and Srivastava, 1983;



405 Gardner and Sharp, 2010). In this study, the effects of BC containments on snow albedo and snow
406 water equivalent (SWE) reduction were estimated.

407

408 Figure 8 shows the calculated the effects of BC containments on annual mean radiative forcing increase
409 (RFI) (W m^{-2}) and snow water equivalent (SWE) reduction (mm yr^{-1} ; millimeter per year), under fresh
410 snow assumption and aged snow assumption. The results show that under the fresh snow assumption
411 (lower limit), the increases of RFI ranged from 0.2 W m^{-2} to 2.5 W m^{-2} , while under the aged snow
412 assumption (upper limit), the increases of RFI ranged from 0.9 W m^{-2} to 5.7 W m^{-2} . This estimate is
413 consistent with the previous studies (Flanner et al., 2009) During the Kuwait fires period, the RFI values
414 increased about 2-5 times higher, which led to a significant increase for the snow melting during the
415 period.

416

417 The runoff of the melted snow due to the increase of snow surface albedo was estimated in this study.
418 A first-order estimation was based on the additional energy contribution to the snowpack due to BC
419 deposition. First the melting point of snow was estimated. Second, the extra snow melt from light
420 absorbing black carbon was estimated by dividing hourly instantaneous radiative forcing, with the
421 enthalpy of fusion of water at 0°C of $0.334 \times 10^6 \text{ J kg}^{-1}$ (Painter et al., 2013; Kaspari et al., 2015).
422 The estimation represented the snow melt in kg m^{-2} across the hour during acquisition translates, or
423 melt in mm of snow water equivalent (SWE). The melted snow due to the BC water was calculated
424 (shown in Fig. 8). The result shows that the estimated averaged SWE reductions were 111 mm and 270
425 mm, for fresh and aged snow respectively. During the Kuwait fires period, the estimated SWE
426 significantly increased, reaching to 600 mm for aged snow condition, and 300 mm for fresh snow
427 condition. The increase was about 3 times than pre- and post- Kuwait fires, suggesting that this special
428 event had a significant impact on snow melting for the Tibetan glaciers and the water resources in the
429 region.

430 4 Conclusions

431 Black carbon (BC) particles change the radiative balance of the atmosphere by absorbing and scattering
432 solar radiation. As a result, BC deposition on the surface of snow and ice changes the albedo of solar
433 radiation. Albedo change is the key parameter to affect the melting of glacier in Tibetan Plateau. In
434 order to study this effect, two sets of measurements were used to study the variability of BC deposition
435 at Muztagh Ata Mountain, Northern Tibetan Plateau. The measured data included the air samplings of
436 BC particles during 2004-2006 and the ice core drillings of BC deposition during 1986-1994. To
437 identify the effect of BC emissions on the BC deposition in this region, a global chemical
438 transportation model (MOZART-4) was used to analyze the BC transport from the source regions. A
439 radiative transfer model (SNICAR) was used to study the effect of BC deposition on snow albedo.

440

441 The results show some important highlights to reveal the temporal variability of BC deposition and the
442 effect of long-rang transport on the BC pollution in the Northern Tibetan Plateau, which are



443 summarized as the follows;

- 444 (1) During 1991-1992, there was a strong spike of the BC deposition at Muztagh Ata, suggesting
445 that there was unusual emission in the upward region. This high peak of BC deposition was
446 investigated by using the global chemical transportation model (MOZART-4). The analysis
447 indicated that the emissions from large Kuwait fires at the end of the first Gulf War in 1991
448 caused the high peak of the BC concentrations and the BC deposition. As a result, the BC
449 deposition in 1991 and 1992 at the Muztagh Ata Mountain was 3-4 times higher than other
450 periods.
- 451 (2) The effect of Kuwait fires on the BC deposition at the Muztagh Ata Mountain suggested that
452 the upward BC emissions had important impacts on this remote site located in Northern
453 Tibetan Plateau. In order to quantitatively estimate the effect of surrounding emissions on the
454 BC concentrations in the northern Tibetan Plateau, a sensitive study with 4 individual BC
455 emission regions (Central Asia, Europe, Persian Gulf, and South Asia) was conducted by
456 using the MOZART-4 model. The result suggests that during the “normal period” (non Kuwait
457 Fires), the largest effect was due to the Central Asia source (44%) during Indian monsoon
458 period. During non-monsoon period, the largest effect was due to the South Asia source
459 (34%).
- 460 (3) The increase of radiative forcing increase (RFI) due to the deposition of BC on snow was
461 estimated by using the radiative transfer model (SNICAR). The results show that under the
462 fresh snow assumption, the estimated RFI ranged from 0.2 W m^{-2} to 2.5 W m^{-2} , while under
463 the aged snow assumption, the estimated RFI ranged from 0.9 W m^{-2} to 5.7 W m^{-2} . During the
464 Kuwait fires period, the RFI values increased about 2-5 times higher than the “normal period”,
465 suggesting a significant increase for the snow melting in Northern Tibetan Plateau due to this
466 fire event.

467

468 This result suggests that the variability of BC deposition at the Muztagh Ata Mountain provides useful
469 information to study the effect of the upward BC emissions on environmental and climate issues in the
470 Northern Tibetan Plateau. The radiative effect of BC deposition on the snow melting provides
471 important information regarding the water resources in the region.

472

473 **Acknowledgement**

474 This work was supported by the National Natural Science Foundation of China (NSFC) under Grant
475 Nos. 41430424 and 41730108. The Authors thanks the supports of Center for Excellence in Urban
476 Atmospheric Environment, Institute of Urban Environment, Chinese Academy of Sciences. The
477 National Center for Atmospheric Research is sponsored by the National Science Foundation.

478

479

480 **References**

- 481 An, Z. S., Kutzbach, J. E., Prell, W. L., and Porter, S. C.: Evolution of Asian monsoons and phased
482 uplift of the Himalaya-Tibetan plateau since Late Miocene times, *Nature*, 411, 62–66,
483 doi:10.1038/35075035, 2001.
- 484 Bauer, S. E., Bausch, A., Nazarenko, L., Tsigaridis, K., Xu, B., Edwards, R., Bisiaux, M., and
485 McConnell, J.: Historical and future black carbon deposition on the three ice caps: Ice core
486 measurements and model simulations from 1850 to 2100, *J. Geophys. Res. Atmos.*, 118,
487 7948–7961, doi:10.1002/jgrd.50612, 2013.
- 488 Bisiaux, M. M., Edwards, R., McConnell, J. R., Curran, M. A. J., van Ommen, T. D., Smith, A. M.,
489 Neumann, T. A., Pasteris, D. R., Penner, J. E., and Taylor, K.: Changes in black carbon deposition
490 to Antarctica from two high-resolution ice core records, 1850–2000 AD, *Atmos. Chem. Phys.*, 12,
491 4107–4115, doi:10.5194/acp-12-4107-2012, 2012.
- 492 Bond, T. C. and Bergstrom, R. W.: Light Absorption by Carbonaceous Particles: An Investigative
493 Review, *Aerosol Sci. Tech.*, 40, 27–67, doi:10.1080/02786820500421521, 2006.
- 494 Bond, T. C., Bhardwaj, E., Dong, R., Jogani, R., Jung, S., Roden, C., Streets, D. G., and Trautmann, N.
495 M.: Historical emissions of black and organic carbon aerosol from energy-related combustion,
496 1850–2000, *Global Biogeochem. Cycles*, 21, n/a-n/a, doi:10.1029/2006GB002840, 2007.
- 497 Bond, T. C., Streets, D. G., Yarber, K. F., Nelson, S. M., Woo, J.-H., and Klimont, Z.: A
498 technology-based global inventory of black and organic carbon emissions from combustion, *J.*
499 *Geophys. Res.*, 109, 1042, doi:10.1029/2003JD003697, 2004.
- 500 Brasseur, G. P., Hauglustaine, D. A., Walters, S., Rasch, P. J., Müller, J.-F., Granier, C., and Tie, X. X.:
501 MOZART, a global chemical transport model for ozone and related chemical tracers: I. Model
502 description, *J. Geophys. Res.*, 103, 28265–28289, doi:10.1029/98JD02397, 1998.
- 503 Cao, J. J., Lee, S. C., Ho, K. F., Zhang, X. Y., Zou, S. C., Fung, K., Chow, J. C., and Watson, J. G.:
504 Characteristics of carbonaceous aerosol in Pearl River Delta Region, China during 2001 winter
505 period, *Atmos. Environ.*, 37, 1451–1460, doi:10.1016/S1352-2310(02)01002-6, 2003.
- 506 Cao, J. J., Xu, B. Q., He, J. Q., Liu, X. Q., Han, Y. M., Wang, G. H., and Zhu, C. S.: Concentrations,
507 seasonal variations, and transport of carbonaceous aerosols at a remote Mountainous region in
508 western China, *Atmos. Environ.*, 43, 4444–4452, 2009.
- 509 Chang, L. Y., Xu, J. M., Tie, X. X., and Wu, J. B.: Impact of the 2015 El Nino event on winter air
510 quality in China, *Sci. Rep.*, 6, 34275, doi:10.1038/srep34275, 2016.
- 511 Chen, Y., Yang, K., He, J., Qin, J., Shi, J., Du, J., and He, Q.: Improving land surface temperature
512 modeling for dry land of China, *J. Geophys. Res.*, 116, 251, doi:10.1029/2011JD015921, 2011.
- 513 Chow, J. C., Watson, J. G., Chen, L. W. A., Arnott, W. P., Moosmüller, H., and Fung, K.: Equivalence
514 of elemental carbon by thermal/optical reflectance and transmittance with different temperature
515 protocols, *Environ. Sci. Technol.*, 38, 4414–4422, 2004.
- 516 Chow, J. C., Watson, J. G., Pritchett, L. C., Pierson, W. R., Frazier, C. A., and Purcell, R. G.: The dri
517 thermal/optical reflectance carbon analysis system: Description, evaluation and applications in U.S.
518 Air quality studies, *Atmos. Environ. Part A. General Topics.*, 27, 1185–1201,



- 519 doi:10.1016/0960-1686(93)90245-T, 1993.
- 520 Conway, H., Gades, A., and Raymond, C. F.: Albedo of dirty snow during conditions of melt, *Water*
521 *Resour. Res.*, 32, 1713–1718, doi:10.1029/96WR00712, 1996.
- 522 Cooke, W. F. and Wilson, J. J. N.: A global black carbon aerosol model, *J. Geophys. Res.*, 101,
523 19395–19409, doi:10.1029/96JD00671, 1996.
- 524 Emmons, L. K., Walters, S., Hess, P. G., Lamarque, J.-F., Pfister, G. G., Fillmore, D., Granier, C.,
525 Guenther, A., Kinnison, D., Laepple, T., Orlando, J., Tie, X., Tyndall, G., Wiedinmyer, C.,
526 Baughcum, S. L., and Kloster, S.: Description and evaluation of the Model for Ozone and Related
527 chemical Tracers, version 4 (MOZART-4), *Geosci. Model Dev.*, 3, 43–67,
528 doi:10.5194/gmd-3-43-2010, 2010.
- 529 Fang, Y., Chen, Y. J., Tian, C. G., Lin, T., Hu, L. M., Huang, G. P., Tang, J. H., Li, J., and Zhang, G.:
530 Flux and budget of BC in the continental shelf seas adjacent to Chinese high BC emission source
531 regions, *Global Biogeochem. Cycles*, 29, 957–972, doi:10.1002/2014GB004985, 2015.
- 532 Flanner, M. G. and Zender, C. S.: Snowpack radiative heating: Influence on Tibetan Plateau climate,
533 *Geophys. Res. Lett.*, 32, 10,219, doi:10.1029/2004GL022076, 2005.
- 534 Flanner, M. G., Zender, C. S., Hess, P. G., Mahowald, N. M., Painter, T. H., Ramanathan, V., and Rasch,
535 P. J.: Springtime warming and reduced snow cover from carbonaceous particles, *Atmos. Chem.*
536 *Phys.*, 9, 2481–2497, doi:10.5194/acp-9-2481-2009, 2009.
- 537 Flanner, M. G., Zender, C. S., Randerson, J. T., and Rasch, P. J.: Present-day climate forcing and
538 response from black carbon in snow, *J. Geophys. Res.*, 112, 3131, doi:10.1029/2006JD008003,
539 2007.
- 540 Gardner, A. S. and Sharp, M. J.: A review of snow and ice albedo and the development of a new
541 physically based broadband albedo parameterization, *J. Geophys. Res.*, 115, D13203,
542 doi:10.1029/2009JF001444, 2010.
- 543 Hack, J. J.: Parameterization of moist convection in the National Center for Atmospheric Research
544 community climate model (CCM2), *J. Geophys. Res.*, 99, 5551, doi:10.1029/93JD03478, 1994.
- 545 Hagen, D. E., Trueblood, M. B., and Whitefield, P. D.: A Field Sampling of Jet Exhaust Aerosols,
546 *Particulate Sc. & Tech.*, 10, 53–63, doi:10.1080/02726359208906598, 1992.
- 547 Hansen, J. and Nazarenko, L.: Soot climate forcing via snow and ice albedos, *P. Natl. Acad. Sci. USA*,
548 101, 423–428, 2004.
- 549 Hobbs, P. V. and Radke, L. F.: Airborne studies of the smoke from the kuwait oil fires, *Science*, 256,
550 987–991, doi:10.1126/science.256.5059.987, 1992.
- 551 Holben, B. N., Eck, T. F., Slutsker, I., Tanré, D., Buis, J. P., Setzer, A., Vermote, E., Reagan, J. A.,
552 Kaufman, Y. J., Nakajima, T., Lavenu, F., Jankowiak, I., and Smirnov, A.: AERONET—A
553 Federated Instrument Network and Data Archive for Aerosol Characterization, *Remote Sens.*
554 *Environ.*, 66, 1–16, doi:10.1016/S0034-4257(98)00031-5, 1998.
- 555 Holtzlag, A. A. M. and Boville, B. A.: Local Versus Nonlocal Boundary-Layer Diffusion in a Global
556 Climate Model, *J. Climate*, 6, 1825–1842, 1993.
- 557 Jurado, E., Dachs, J., Duarte, C. M., and Simó, R.: Atmospheric deposition of organic and black carbon
558 to the global oceans, *Atmos. Environ.*, 42, 7931–7939, doi:10.1016/j.atmosenv.2008.07.029, 2008.



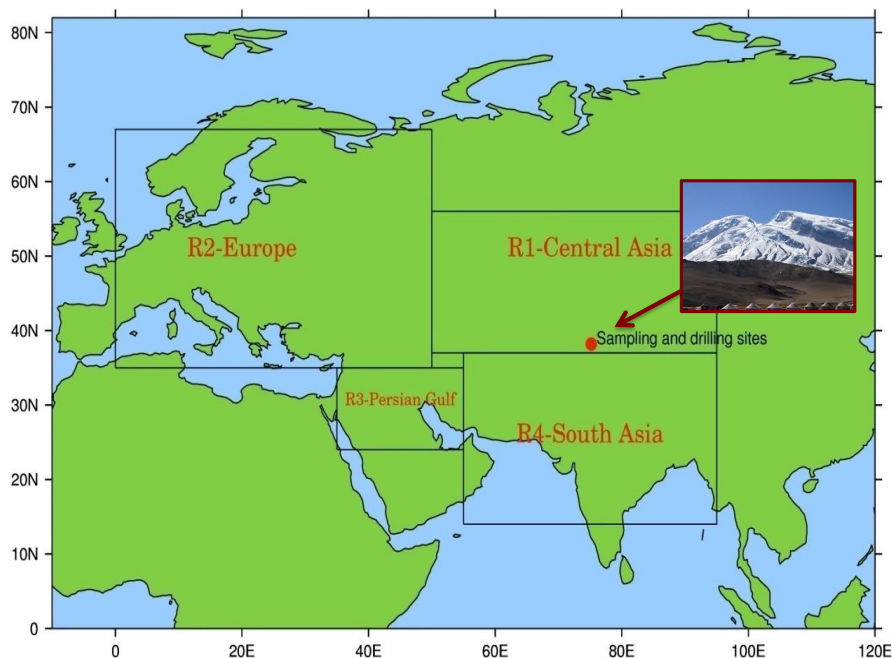
- 559 Jurado, E., Jaward, F., Lohmann, R., Jones, K. C., Simó R., and Dachs, J.: Wet Deposition of Persistent
560 Organic Pollutants to the Global Oceans, *Environ. Sci. Technol.*, 39, 2426–2435,
561 doi:10.1021/es048599g, 2005.
- 562 Kaspari, S., McKenzie Skiles, S., Delaney, I., Dixon, D., and Painter, T. H.: Accelerated glacier melt on
563 Snow Dome, Mount Olympus, Washington, USA, due to deposition of black carbon and mineral
564 dust from wildfire, *J. Geophys. Res. Atmos.*, 120, 2793–2807, doi:10.1002/2014JD022676, 2015.
- 565 Kaspari, S. D., Schwikowski, M., Gysel, M., Flanner, M. G., Kang, S., Hou, S., and Mayewski, P. A.:
566 Recent increase in black carbon concentrations from a Mt. Everest ice core spanning 1860–2000
567 AD, *Geophys. Res. Lett.*, 38, n/a–n/a, doi:10.1029/2010GL046096, 2011.
- 568 Kinnison, D. E., Brasseur, G. P., Walters, S., Garcia, R. R., Marsh, D. R., Sassi, F., Harvey, V. L.,
569 Randall, C. E., Emmons, L., Lamarque, J. F., Hess, P., Orlando, J. J., Tie, X. X., Randel, W., Pan, L.
570 L., Gettelman, A., Granier, C., Diehl, T., Niemeier, U., and Simmons, A. J.: Sensitivity of chemical
571 tracers to meteorological parameters in the MOZART-3 chemical transport model, *J. Geophys. Res.*,
572 112, 32295, doi:10.1029/2006JD007879, 2007.
- 573 Lavanchy, V.M.H., Gäggeler, H. W., Schotterer, U., Schwikowski, M., and Baltensperger, U.: Historical
574 record of carbonaceous particle concentrations from a European high-alpine glacier (Colle Gnifetti,
575 Switzerland), *J. Aerosol Sci.*, 30, S611–S612, doi:10.1016/S0021-8502(99)80316-4, 1999.
- 576 Li, C. L., Yan, F. P., Kang, S. C., Chen, P. F., Han, X. W., Hu, Z. F., Zhang, G. S., Hong, Y., Gao, S. P.,
577 Qu, B., Zhu, Z. J., Li, J. W., Chen, B., and Sillanpää M.: Re-evaluating black carbon in the
578 Himalayas and the Tibetan Plateau: Concentrations and deposition, *Atmos. Chem. Phys.*, 17,
579 11899–11912, doi:10.5194/acp-17-11899-2017, 2017.
- 580 Lin, S.-J. and Rood, R. B.: Multidimensional Flux-Form Semi-Lagrangian Transport Schemes, *Mon.*
581 *Wea. Rev.*, 124, 2046–2070, 1996.
- 582 Lioussé, C., Cachier, H., and Jennings, S. G.: Optical and thermal measurements of black carbon
583 aerosol content in different environments: Variation of the specific attenuation cross-section, sigma
584 (σ), *Atmospheric Environment. Part A. General Topics*, 27, 1203–1211,
585 doi:10.1016/0960-1686(93)90246-U, 1993.
- 586 Liu, X. Q., Xu, B. Q., Yao, T. D., Wang, N. L., and Wu, G. J.: Carbonaceous particles in Muztagh Ata
587 ice core, West Kunlun Mountains, China, *Sci. Bull.*, 53, 3379–3386,
588 doi:10.1007/s11434-008-0294-5, 2008.
- 589 Mackay, D., Paterson, S., and Schroeder, W. H.: Model describing the rates of transfer processes of
590 organic chemicals between atmosphere and water, *Environ. Sci. Technol.*, 20, 810–816,
591 doi:10.1021/es00150a009, 1986.
- 592 McConnell, J. R., Edwards, R., Kok, G. L., Flanner, M. G., Zender, C. S., Saltzman, E. S., Banta, J. R.,
593 Pasteris, D. R., Carter, M. M., and Kahl, J. D. W.: 20th-century industrial black carbon emissions
594 altered Arctic climate forcing, *Science*, 317, 1381–1384, doi:10.1126/science.1144856, 2007.
- 595 Ming, J., Cachier, H., Xiao, C., Qin, D., Kang, S., Hou, S., and Xu, J.: Black carbon record based on a
596 shallow Himalayan ice core and its climatic implications, *Atmos. Chem. Phys.*, 8, 1343–1352,
597 doi:10.5194/acp-8-1343-2008, 2008.
- 598 Nair, V. S., Babu, S. S., Moorthy, K. K., Sharma, A. K., Marinoni, A., and Ajai: Black carbon aerosols



- 599 over the Himalayas: Direct and surface albedo forcing, *Tellus B*, 65, 19738,
600 doi:10.3402/tellusb.v65i0.19738, 2013.
- 601 Painter, T. H., Seidel, F. C., Bryant, A. C., McKenzie Skiles, S., and Rittger, K.: Imaging spectroscopy
602 of albedo and radiative forcing by light-absorbing impurities in mountain snow, *J. Geophys. Res.*
603 *Atmos.*, 118, 9511–9523, doi:10.1002/jgrd.50520, 2013.
- 604 Parungo, F., Nagamoto, C., Zhou, M.-Y., Hansen, A. D.A., and Harris, J.: Aeolian transport of aerosol
605 black carbon from Aeolian transport of aerosol black carbon from China to the ocean, *Atmos.*
606 *Environ.*, 28, 3251–3260, 1994.
- 607 Petr Chylek, V. R. and Srivastava, V.: Albedo of soot-contaminated snow, *J. Geophys. Res.*, 88,
608 10837–10843, 1983.
- 609 Petzold, A., Ogren, J. A., Fiebig, M., Laj, P., Li, S.-M., Baltensperger, U., Holzer-Popp, T., Kinne, S.,
610 Pappalardo, G., Sugimoto, N., Wehrli, C., Wiedensohler, A., and Zhang, X.-Y.: Recommendations
611 for reporting "black carbon" measurements, *Atmos. Chem. Phys.*, 13, 8365–8379,
612 doi:10.5194/acp-13-8365-2013, 2013.
- 613 Ramanathan, V., Crutzen, P. J., Kiehl, J. T., and Rosenfeld, D.: Aerosols, climate, and the hydrological
614 cycle, *Science*, 294, 2119–2124, 2001.
- 615 Rasch, P. J., Mahowald, N. M., and Eaton, B. E.: Representations of transport, convection, and the
616 hydrologic cycle in chemical transport models: Implications for the modeling of short-lived and
617 soluble species, *J. Geophys. Res.*, 102, 28,127–28,138, 1997.
- 618 Schwarz, J. P., Gao, R. S., Fahey, D. W., Thomson, D. S., Watts, L. A., Wilson, J. C., Reeves, J. M.,
619 Darbeheshti, M., Baumgardner, D. G., Kok, G. L., Chung, S. H., Schulz, M., Hendricks, J., Lauer,
620 A., Kärcher, B., Slowik, J. G., Rosenlof, K. H., Thompson, T. L., Langford, A. O., Loewenstein, M.,
621 and Aikin, K. C.: Single-particle measurements of midlatitude black carbon and light-scattering
622 aerosols from the boundary layer to the lower stratosphere, *J. Geophys. Res.*, 111, 2845,
623 doi:10.1029/2006JD007076, 2006.
- 624 Tie, X. X., Madronich, S., Walters, S., Edwards, D. P., Ginoux, P., Mahowald, N., Zhang, R. Y., Lou, C.,
625 and Brasseur, G.: Assessment of the global impact of aerosols on tropospheric oxidants, *J. Geophys.*
626 *Res.*, 110, 13,791, doi:10.1029/2004JD005359, 2005.
- 627 Wang, M., Xu, B., Cao, J., Tie, X., Wang, H., Zhang, R., Qian, Y., Rasch, P. J., Zhao, S., Wu, G., Zhao,
628 H., Joswiak, D. R., Li, J., and Xie, Y.: Carbonaceous aerosols recorded in a southeastern Tibetan
629 glacier: Analysis of temporal variations and model estimates of sources and radiative forcing,
630 *Atmos. Chem. Phys.*, 15, 1191–1204, doi:10.5194/acp-15-1191-2015, 2015a.
- 631 Wang, M., Xu, B. Q., Kaspari, S. D., Gleixner, G., Schwab, V. F., Zhao, H. B., Wang, H. L., and Yao, P.:
632 Century-long record of black carbon in an ice core from the Eastern Pamirs: Estimated
633 contributions from biomass burning, *Atmos. Environ.*, 115, 79–88,
634 doi:10.1016/j.atmosenv.2015.05.034, 2015b.
- 635 Warren, S. G. and Wiscombe, W. J.: A Model for the Spectral Albedo of Snow. II: Snow Containing
636 Atmospheric Aerosols, *J. Atmos. Sci.*, 37, 2734–2745, 1980.
- 637 Wendl, I. A., Menking, J. A., Färber, R., Gysel, M., Kaspari, S. D., Laborde, M. J. G., and Schwikowski,
638 M.: Optimized method for black carbon analysis in ice and snow using the Single Particle Soot



- 639 Photometer, Atmos. Meas. Tech., 7, 2667–2681, doi:10.5194/amt-7-2667-2014, 2014.
- 640 Wiscombe, W. J. and Warren, S. G.: A Model for the Spectral Albedo of Snow. I: Pure Snow, J. Atmos.
641 Sci., 37, 2712–2733, 1980.
- 642 Wu, G. J., Yao, T. D., Xu, B. Q., Li, Z., Tian, L. D., Duan, K. Q., and Wen, L. K.: Grain size record of
643 microparticles in the Muztagata ice core, Sci. China Ser. D, 49, 10–17,
644 doi:10.1007/s11430-004-5093-5, 2006.
- 645 Wu, G. J., Yao, T. D., Xu, B. Q., Tian, L. D., Li, Z., and Duan, K. Q.: Seasonal variations of dust record
646 in the Muztagata ice cores, Sci. Bull., 53, 2506–2512, doi:10.1007/s11434-008-0197-5, 2008.
- 647 Xu, B., Cao, J., Hansen, J., Yao, T., Joswiak, D. R., Wang, N., Wu, G., Wang, M., Zhao, H., Yang, W.,
648 Liu, X., and He, J.: Black soot and the survival of Tibetan glaciers, P. Natl. Acad. Sci. USA, 106,
649 22114–22118, doi:10.1073/pnas.0910444106, 2009a.
- 650 Xu, B. Q., Wang, M., Joswiak, D. R., Cao, J. J., Yao, T. D., Wu, G. J., Yang, W., and Zhao, H. B.:
651 Deposition of anthropogenic aerosols in a southeastern Tibetan glacier, J. Geophys. Res., 114, 9185,
652 doi:10.1029/2008JD011510, 2009b.
- 653 Yasunari, T. J., Bonasoni, P., Laj, P., Fujita, K., Vuillermoz, E., Marinoni, A., Cristofanelli, P., Duchi, R.,
654 Tartari, G., and Lau, K.-M.: Estimated impact of black carbon deposition during pre-monsoon
655 season from Nepal Climate Observatory – Pyramid data and snow albedo changes over Himalayan
656 glaciers, Atmos. Chem. Phys., 10, 6603–6615, doi:10.5194/acp-10-6603-2010, 2010.
- 657 Yasunari, T. J., Tan, Q., Lau, K.-M., Bonasoni, P., Marinoni, A., Laj, P., Mánéguez, M., Takemura, T.,
658 and Chin, M.: Estimated range of black carbon dry deposition and the related snow albedo
659 reduction over Himalayan glaciers during dry pre-monsoon periods, Atmos. Environ., 78, 259–267,
660 doi:10.1016/j.atmosenv.2012.03.031, 2013.
- 661 Zhang, G. J. and McFarlane, N. A.: Sensitivity of climate simulations to the parameterization of
662 cumulus convection in the Canadian climate centre general circulation model, Atmos. Ocean, 33,
663 407–446, doi:10.1080/07055900.1995.9649539, 1995.
- 664 Zhao, H. B., Xu, B. Q., Yao, T. D., Tian, L. D., and Li, Z.: Records of sulfate and nitrate in an ice core
665 from Mount Muztagata, central Asia, J. Geophys. Res., 116, 275, doi:10.1029/2011JD015735,
666 2011.
- 667 Zhao, Z., Cao, J., Shen, Z., Xu, B., Zhu, C., Chen, L.-W. A., Su, X., Liu, S., Han, Y., Wang, G., and Ho,
668 K.: Aerosol particles at a high-altitude site on the Southeast Tibetan Plateau, China: Implications
669 for pollution transport from South Asia, J. Geophys. Res. Atmos., 118, 11,360–11,375,
670 doi:10.1002/jgrd.50599, 2013.
- 671

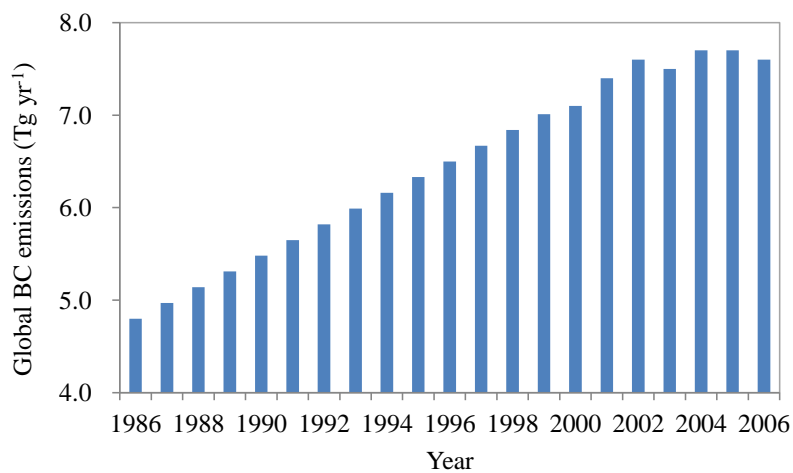


672

673

674

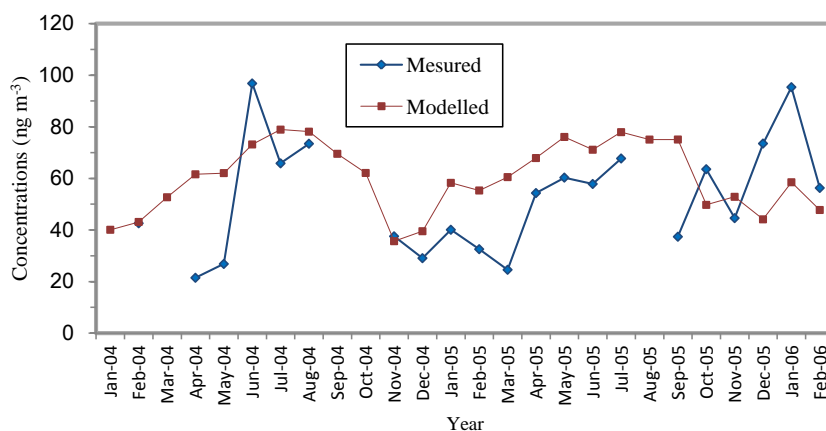
Fig 1. The Muztagh Ata measurement site (indicated by the red dot), and the surrounding BC source areas (R1-Central Asia region; R2-European region; R3-Persian Gulf region; and R4-South Asia region).



675

676

Fig 2. The trend of global BC emission (Tg/yr) from 1986 to 2006 used in this study

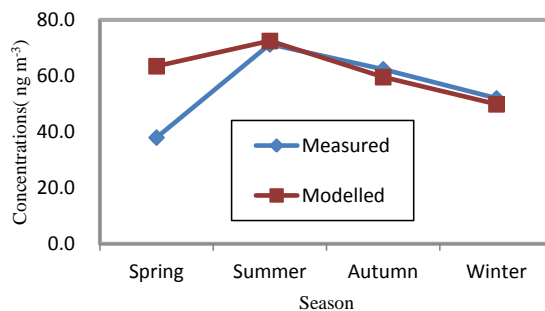


677

678 **Fig 3a. Comparison of calculated (red) and measured (blue) monthly mean BC concentrations at the surface**
679 **level during Jan. 2004 to Feb. 2006 measured by the Cold and Arid Regions Environmental and**
680 **Engineering Institute, Chinese Academy of Sciences.**

681

682

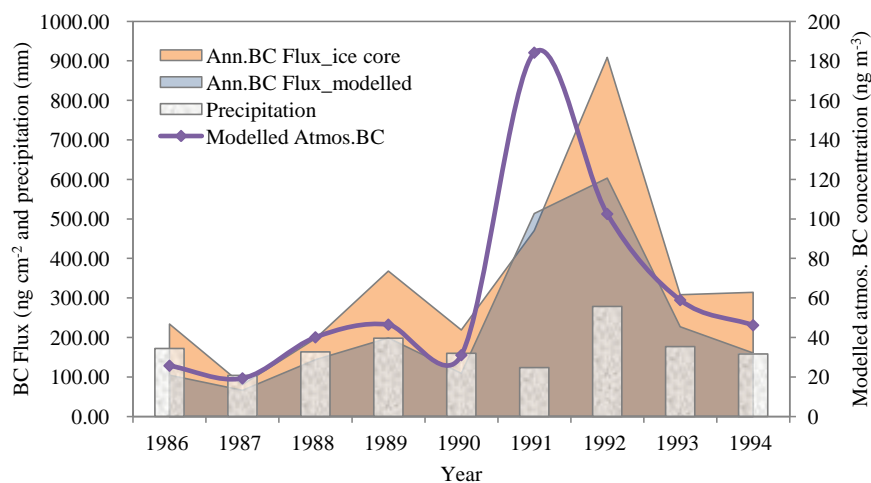


683

684 **Fig 3b. Comparison of calculated (red) and measured (blue) seasonal variation during Jan. 2004 to Feb.**
685 **2006. Spring includes March, April and May in 2004 and 2005. Summer includes June, July and August in**
686 **2004, 2005; Autumn includes September, October and November in 2004, 2005; Winter includes December,**
687 **January and February of 2004, 2005 and January, February in 2006.**

688

689



690

691

692

693

694

Fig 4. Comparison of measured annual BC deposition flux with the model calculation between ice core and simulation, as well as the modelled atmospheric BC concentration and precipitation used for BC deposition flux calculation

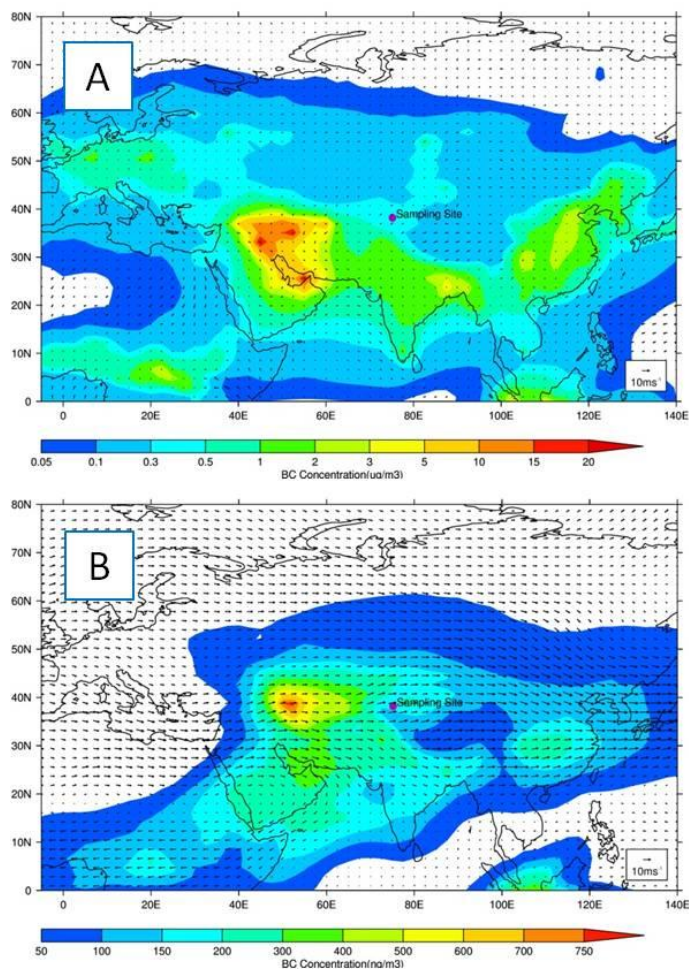


695

696

697

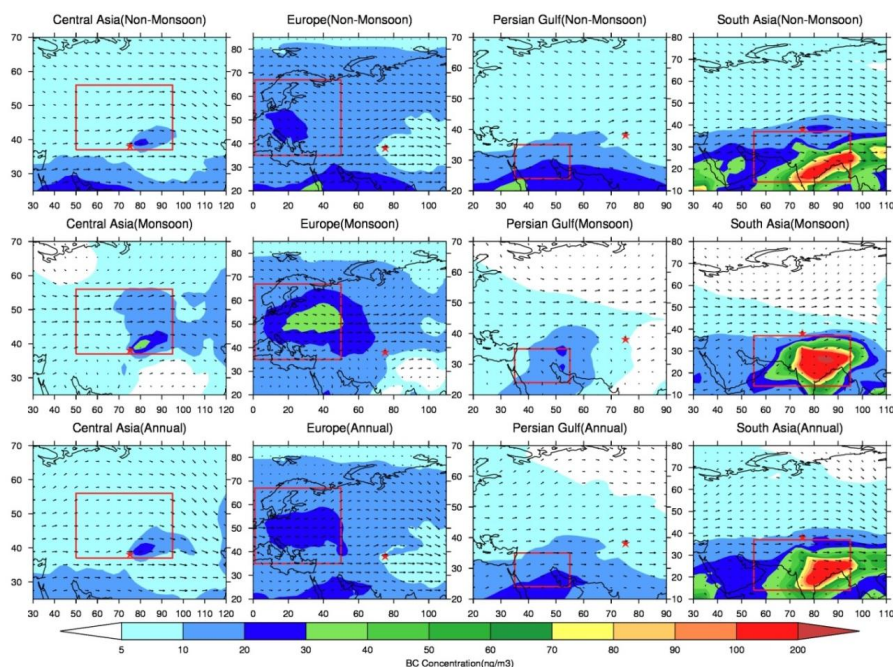
Fig 5. The image of the fires in Kuwait during 1991. It shows the intensive fires and the raise up of plume due to the heat buoyance. The lower panel shows the fires were transported to east due to western winds.



698

699

700 **Fig. 6.** The calculated horizontal distributions of BC concentrations ($\mu\text{g m}^{-3}$) at the surface (A) and the
701 concentrations (ng m^{-3}) at 5 km above the surface (B). The wind direction and speed are indicated by black
702 arrows.



703

704

705

706

707

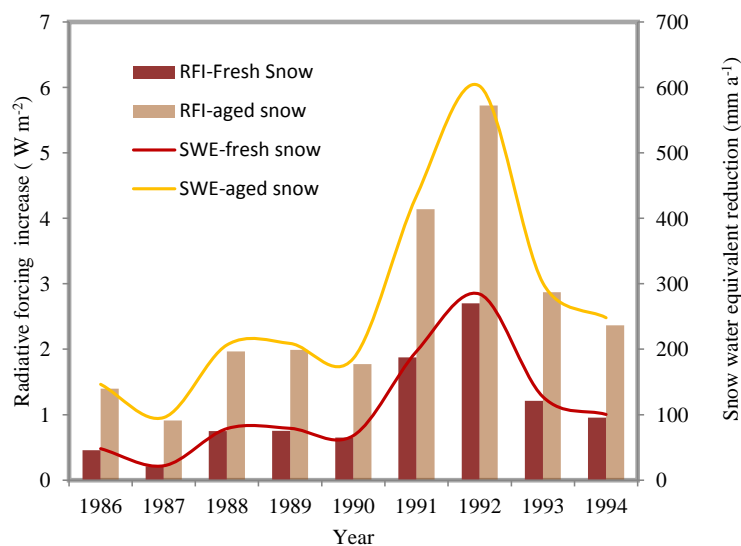
708

709

710

711

Fig 7. The calculated spatial BC distributions due to individual BC from the four source regions (Central Asia, Europe, Persian Gulf and South Asia) above 5 km above the surface during different periods, i.e., monsoon (June-September), non-monsoon (October-May), and annual mean in 1993. The red star is where the study site of Muztagh Ata located. The red boxes indicate the boundary of the four source regions.



712

713 Fig 8. Estimated the effects of BC containments on annual mean radiative forcing increase (RFI) (W/m^2)
 714 and snow water equivalent (SWE) reduction (mm/a), under fresh snow assumption (purple line and bars)
 715 and aged snow assumption (yellow line and bars).

716

717

718 Table 1. Source regions and corresponding fractional contributions to atmospheric BC concentrations at the
 719 Muztagh Ata site in monsoon, non-monsoon and all months during 1993

720

	Source regions	Latitude	Longitude	Summer monsoon (June-September)	Non-monsoon (October-May)	Annual
R1	Central Asia	37-56 °N	50-95 °E	43.9%	18.1%	26.7%
R2	Europe	35-67 °N	0-50 °E	26.6%	11.5%	16.5%
R3	Persian Gulf	24-35 °N	35-55 °E	9.4%	12.1%	11.2%
R4	South Asia	14-37 °N	55-95 °E	7.3%	33.7%	24.9%
	Others	NA	NA	7.9%	6.2%	6.8%

721

722

723

724

725